Materials & Design 223 (2022) 111143

Contents lists available at ScienceDirect

Materials & Design

journal homepage: www.elsevier.com/locate/matdes

Prognostics and health management of composite structures under multiple impacts through electromechanical behavior and a particle filter

In-Yong Lee [a], Hyung Doh Roh [b], Young-Bin Park [a,*]

[a] Department of Mechanical Engineering, Ulsan National Institute of Science and Technology, UNIST-gil 50, Ulju-gun, Ulsan 44919, Republic of Korea
[b] Carbon Composites Department, Composites Research Division, Korea Institute of Materials Science (KIMS), Changwon, Gyeongnam 51508, Republic of Korea

HIGHLIGHTS

- Advanced real-time condition-based monitoring methodology is proposed using electromechanical behavior data and sequential Monte Carlo algorithms.
- Proposed methodology overcomes the limitations of previous real-time prognostics self-sensing research under repeated impacts.
- Damage states with various types of damage were monitored in real time using electromechanical behavior under multiple impacts.
- Damage status and remaining number of useful impacts were predicted real-time using particle filter within a 10% error.
- Applicability was confirmed by monitoring and predicting the health state of a wind-turbine blade under multiple impacts.

GRAPHICAL ABSTRACT

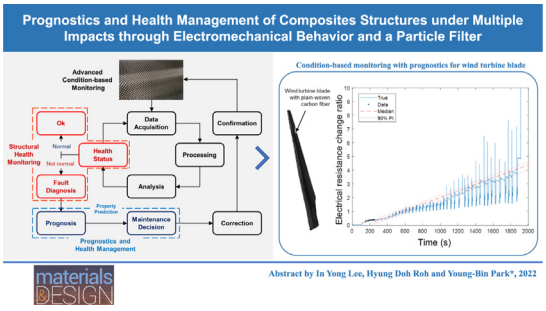

ARTICLE INFO

Article history:
Received 9 May 2022
Revised 9 September 2022
Accepted 9 September 2022
Available online 13 September 2022

Keywords:
Polymer–matrix composites
Smart materials
Nondestructive evaluation

ABSTRACT

Self-sensing techniques are restricted to monitoring the various types of damage caused during repeated impact testing, and only a few studies have investigated the prognostics of carbon fiber reinforced plastics (CFRPs); in these studies, the electrical resistance of CFRPs was gauged in real time during multiple-impact testing. Therefore, real-time prognostics and health management using electromechanical behavior data obtained from CFRP structures under repeated impact testing are proposed herein. The health condition of the CFRP is observed in real time during impact testing using mechanical and electromechanical behavior data. Further, the types of failure observed during impact testing are investigated using real-time self-sensing data. Moreover, a particle filter is used for predicting the electromechanical behavior and the remaining number of useful impacts during repeated impact testing conducted using a physics-based prognostics tool. The applicability of the proposed methodology was confirmed by monitoring and predicting impact damage growth on the wind-turbine blade within a 5% prediction error. An advanced-condition-

* Corresponding author.
E-mail address: ypark@unist.ac.kr (Y.-B. Park).

https://doi.org/10.1016/j.matdes.2022.111143
0264-1275/

based monitoring technique with the diagnostics and prognostics of the current health state was designed successfully, and an application of the introduced method was demonstrated for industrial use.

1. Introduction

Carbon fiber reinforced plastic (CFRP) has become considerably popular in several industries. Structures built using CFRP are widely used in wind-turbine blades, for which lightweight and high-specific-strength material is suitable. In the wind-turbine system industry, wind-turbine blades measuring over 60 m are manufactured using carbon fiber for increasing the energy efficiency and reducing the weight [1–3]. However, the wind-turbine system suffers from several challenges—it is exposed easily to mechanical impact such as storms, bird strikes, hail, and other types of mechanical strikes [4–6]. Structural health monitoring (SHM) in CFRP structures has been studied under impact conditions using nondestructive evaluation (NDE) methods such as eddy currents, acoustic emissions, and fiber Bragg grating sensors [7–12]. The SHM and prognostics and health management (PHM) of CFRP is conducted using the piezoresistive effect, which generates a change in electrical resistivity when a structure is subjected to mechanical strain. This NDE technique helps in real-time SHM because extra sensors are not required, and it incurs a low cost for SHM. To date, several self-sensing techniques under impact testing conditions have been reported [13–17]; however, limited studies have analyzed the various types of damages caused in CFRP and focused on the prediction of electromechanical behavior.

The PHM of material property prediction and the remaining useful lifetime (RUL) calculation have been studied extensively. Two types of prognostic methods are used: data-driven and physics-based. In the former, recurrent [18–20] and convolutional neural networks [21–23] are utilized for PHM. Several Monte-Carlo-based, that is, physics-based, prognostic studies on composite structures have also been reported [24–26]. In addition, several other studies have reported on nondestructive evaluation (NDE) prognostics performed using data-driven and multimodal-based approaches [27–29]. Multisensor NDE and multimodal prognosis methods have been used for assessing the fatigue life in glass-fiber-reinforced plastic (GFRP) composite structures in a reliable manner. Most previous studies have utilized data from sensors such as acoustic emission, lead zirconate titanate (PZT), and strain gauges. However, studies that focus on the life prediction and prognostics of CFRP using self-sensing data remain deficient. Further, studies that analyze the impact number under repeated impacts in composites based on electromechanical behavior are limited. Studies that focus on the real-time prediction of material properties and the calculation of the remaining number of useful impacts using electromechanical behavior data also remain limited.

A real-time advanced-condition-based maintenance (CBM +), which includes SHM and PHM, using electromechanical behavior data is introduced in this study. The structural health status of CFRP structures is observed in real time using self-sensing data under multiple-impact testing. Various types of damage are investigated during repeated impact testing using electromechanical data. For the PHM of CFRP structures, the particle filter (PF) is used to predict the electromechanical behavior and the remaining number of useful impacts during impact testing in real time. The applicability of the proposed CBM + is verified by investigating the three-dimensional (3D) shape of the wind-turbine blade. Further, a scaled-down blade is manufactured using vacuum-assisted resin transfer molding (VARTM). The self-sensing data are obtained from the wind blade under repeated impacts. The proposed CBM + with real-time NDE technique is investigated to analyze the health status and various damages in the composites; it can predict the health condition of the structures. In this study, the applicability of the CBM + technique to the investigation of various types of damage in composite structures in various industries is verified.

2. Experimental

2.1. Materials

A 3 K plain shaped carbon fiber (CF) fabric (Mitsubishi, Japan) was obtained from Jet Korea Corp. (Changwon, Korea) with a thickness and density of 0.2 mm and 305 g/m^2, respectively. Vinylester (RF-1001MV, Epovia, Korea) comprising 45% styrene and 55% epoxy acrylate and a curing agent (Arkema Corp., USA) comprising methyl ethyl ketone peroxide were blended in a 1.0% weight ratio of the vinylester resin. The electrode on the CF fabric was embedded with a 30 AWG (0.25 mm) copper wire and silver paste (P-100, Elcoat, USA). The copper wire has a small diameter to avoid affecting the fractures in the CFRP during the repeated impacts. A quick-epoxy adhesive (Mississauga, Canada) was applied on the parts of the blade for bonding.

2.2. Sample preparation

A 150 mm × 100 mm × 4.5 mm CFRP specimen with 20 plies was manufactured using VARTM as illustrated in Fig. 1(a). The CFs were laid on a mold, and four electrodes were embedded on the CFs, as illustrated in Fig. 1(a). Instead of the woven shape of the CF, unidirectional (UD) CF could also be used for real-time condition-based prognostics. However, UD CF exhibits directionality of electrical conductivity (high electrical conductivity along the fiber direction and low electrical conductivity in the direction horizontal to the fiber direction). Therefore, the sensitivity of composite structures could vary based on the stacking sequence of the UD CF. Silver paste was used to minimize the contact resistance at the electrodes during the measurement of the electrical resistance. The electrodes on the carbon fiber textile were embedded using 30 AWG (0.25 mm diameter) copper wires; this diameter was exceedingly small to minimize any effect on the crack or initiation point in the CFRP during impact testing.

To verify the proposed CBM + system, a 3-kW wind-turbine blade, with a scale-down ratio of 4:1, was manufactured using 10 plies of the CFs (Fig. 1(b)) using VARTM; the dimensions were 80 × 505 × 2.5 mm. The lower and upper molds were manufactured through CNC machining and reverse engineering surface techniques. Four electrodes were installed on the upper part of the blade using the silver paste. The lower and upper parts of the blade were cropped following VARTM manufacturing. Epoxy adhesive was spread on the lower part of the wind blade. Thereafter, it was bonded and cured with the upper part for 5 min.

2.3. Test setup for repeated impacts

Repeated impacts were conducted to investigate the electromechanical behavior of CFRP and the wind-turbine blade using a CEAST 9350 drop-weight impact tester. Two different impact levels (multiple 8- and 9-J impacts) were loaded on the 20-ply CFRP sam-

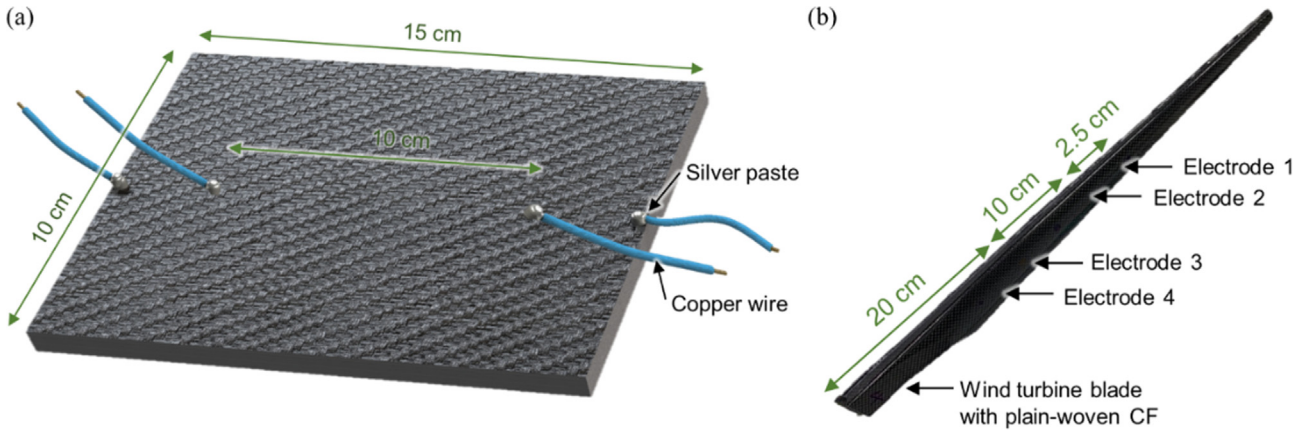

Fig. 1. (a) Schematic of CFRP sample with four electrodes used for impact testing and (b) wind-turbine blade sample.

ple. The scaled-down carbon-fiber-based wind blade was subjected to multiple 4- and 5-J impacts using a CEAST 9350 drop-weight impact tester. Multiple impacts were conducted in the composite structures at the middle of the electrodes. Two guide supports were used for fixing the scaled-down blade and preventing rebound of the composite structures during the multiple-impact testing. If higher energy levels were set, less than 20 impacts would need to be exerted on the composite structures. This implies that the prognostic studies would be conducted with 20 impacts, which is insignificant for the prediction of an electromechanical property because of the prediction over the foreseeable future or a short time period. When the impact energy levels were lower than these, a significantly higher number of impacts (>200 times) would have to be exerted on the composite structures to obtain penetration damage states. Therefore, the impact energy levels were optimized to cause puncture failure between 20 and 200 impacts for efficient prognostic studies. C-scan cannot be applied to hollow-shaped or porous structures [34–38]. Therefore, damage identification using scanning-based nondestructive test (NDT) could not be applied in this study because the wind blade was made of hollow composite structures. Damage identification was investigated using real-time electromechanical behavior, mechanical property analyses, and actual photographs of the damaged wind blade. All the CFRP samples were impacted until penetration occurred in the structures.

The dc electrical resistance was measured with a digital multimeter (Keithley 2002, USA) using the four-probe electrical resistance measurement technique for eliminating the contact resistance during repeated impact testing. The photographs of a drop-weight impact tester, data acquisition (DAQ) systems, and a digital multimeter for simultaneous electrical resistance measurement and impact testing are presented in Fig. 2. In addition, the photographs of the experimental setup used for the impact testing of the scaled-down blade are depicted in Fig. 2(b) and 2(c).

2.4. Particle-filter-based prognostics

Particle filter is popularly used in the sequential Monte Carlo methodology, which is referred to as physics-based prognostics. In the PF, the prior for the current step is investigated using the posterior of the previous step when new information from the sensor, utilized for evaluating the likelihood, is calculated from a sensor; the parameters are updated through multiplication with the likelihood.

The PF distribution comprises particles with their own likelihood weight each. Based on the Bayesian theorem, the prior distribution weight of a particle (θ^i) can be calculated as follows:

$$\mathrm{w}\left(\theta^i\right) = \frac{f(\theta^i|y)}{g(\theta^i)} = \frac{f(\theta^i|y)f(\theta^i)}{g(\theta^i)} \tag{1}$$

where $f(\theta^i|y)$ and $g\left(\theta^i\right)$ denote the probability density function values in the importance and the posterior distribution, which is randomly chosen, respectively. In the PF, the weights are renewed whenever new data are observed. The process of the PF is explained below:

Prediction: At the first step (k = 1), all parameters in the n particles are spread with their initial distribution. The prior distributions at the current kth step are calculated based on the posterior distributions at the previous (k – 1)th step.
Update: The degradation states and model parameters are measured based on the likelihood function (y_k), which represents the observed information. Further, y_k and the weight (w_k^i) can be estimated, respectively, assuming that noise is distributed normally as follows:

$$f\left(y_k|z_k^i,\theta_k^i\right) = \frac{1}{\sqrt{2\pi}\sigma}\left[-\frac{1}{2}\frac{y_k - h(z_k^i))^2}{\sigma^2}\right], i = 1, 2, 3, \ldots, \mathrm{n} \tag{2}$$

$$w_k^i = \frac{f\left(y_k|z_k^i,\theta_k^i\right)}{\sum_{j=1}^{n_s} f\left(y_k|z_k^j,\theta_k^j\right)} \tag{3}$$

Models from the previous step are assigned based on their measured weights. The accuracy can decrease as multiple update processes are estimated for the posterior distribution, and it can, in turn, reduce the bounds of distribution by causing the samples to have low weights.

Resampling: Particles in the update are either eliminated or duplicated to ensure particles with identical weights when the model exhibits low or high likelihood values, respectively. Resampling is performed to avoid the degradation of the system; this ensures that all the particles retain the same weight.

The posterior distribution is estimated once these prediction, update, and resampling steps are repeated; thereafter, the last posterior distribution is utilized to estimate the state variables. The schematic for the overall procedure of the PF is presented in Fig. 3.

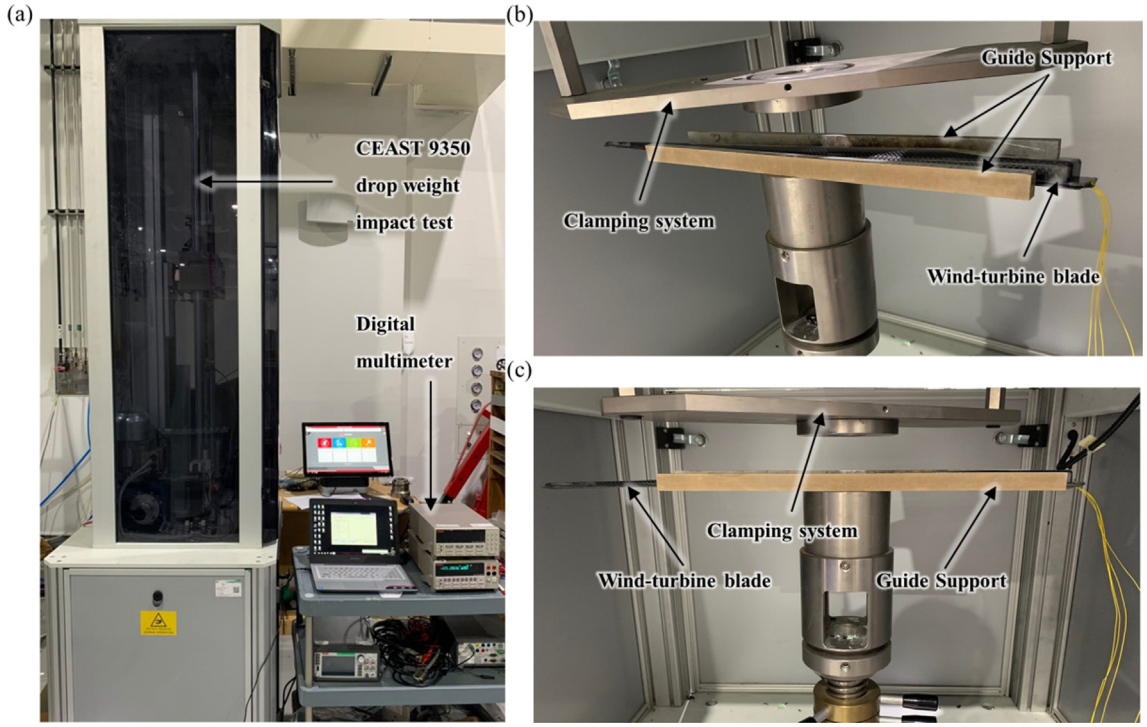

Fig. 2. Experimental setup for simultaneous electrical-resistance-change measurement and impact testing; (b) setup for wind-turbine blade impact testing.

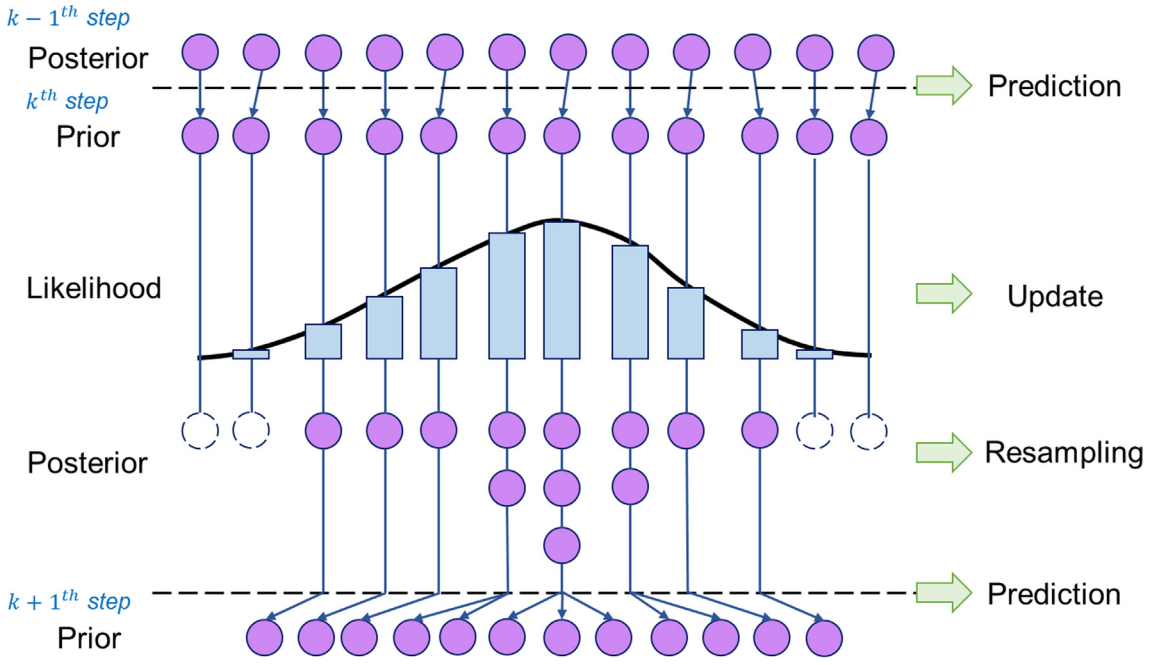

Fig. 3. Schematic for overall procedure of PF.

3. Results and discussion

3.1. Electromechanical behavior analysis in CFRP

Various types of damage were investigated using the mechanical values obtained during the repeated impacts, as depicted in Fig. 4, as referenced in studies on damage analysis under repeated impacts [30–33]. A total of 73 and 68 repeated impacts were exerted with 8- and 9-J step impact energies, respectively. Three different types of damages were investigated in the force and displacement graphs under repeated 8- (Fig. 4(a)) and 9-J (Fig. 4(b)) impacts. Delamination and matrix cracking mainly occurred in the CFRP within the red lines depicted in Fig. 4(a) and 4(b) for a low number of impacts. Fiber breakage started to occur with an increase in the number of impacts at the decreasing and increasing points of the peak force and maximum displacement at the 25th 8-J repeated impact and 23rd 9-J repeated impact, respectively. Fiber breakage occurred and was more severe, as represented by the

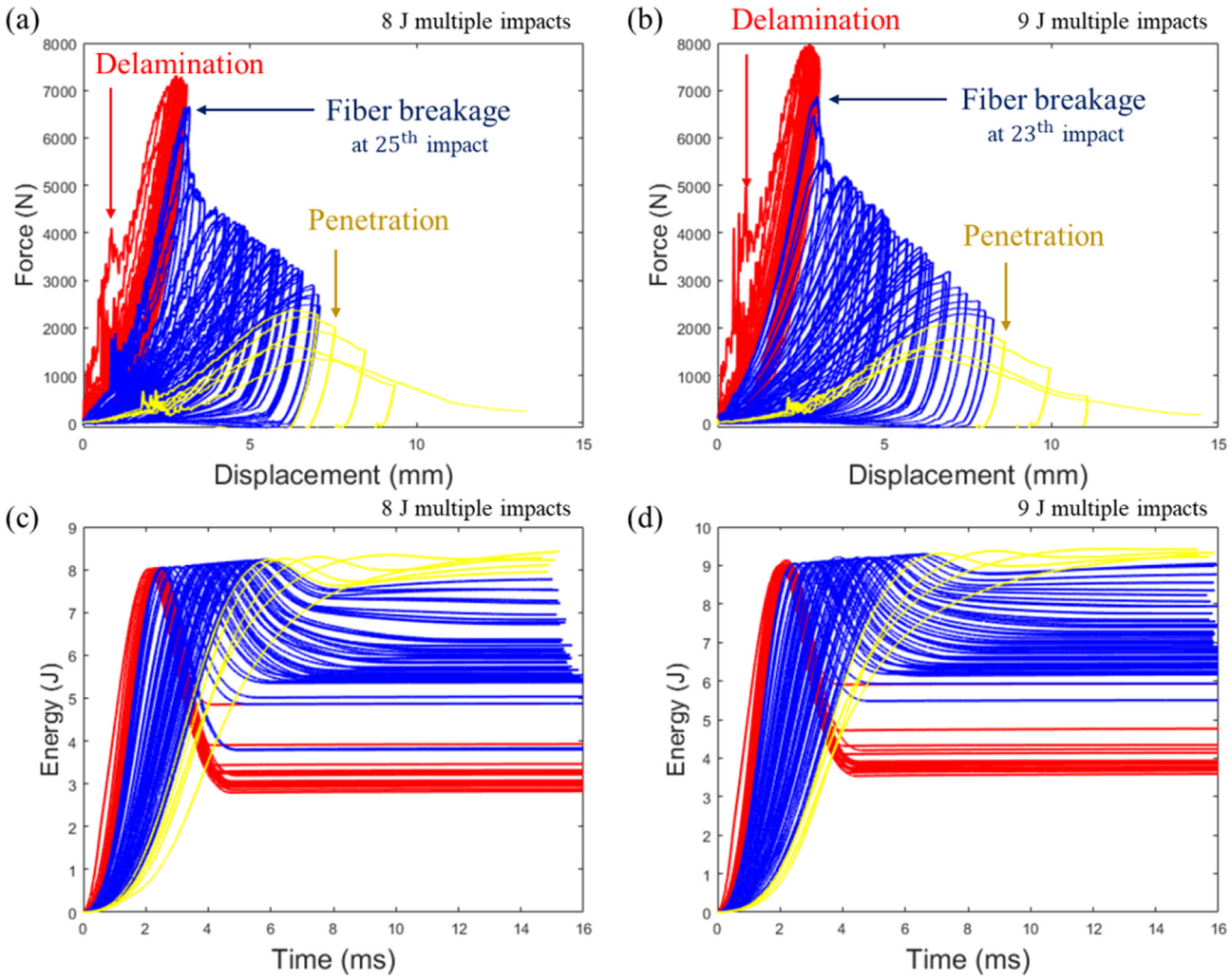

Fig. 4. Force vs displacement graph during (a) 8- and (b) 9-J repeated impacts and energy graphs for multiple (c) 8- and (d) 9-J impacts.

blue lines. Penetration started in the CFRP because the displacement was not recovered during the impact. The penetration occurred within the yellow lines during the repeated impacts. Three different types of damages were investigated, as depicted in the force and displacement graphs, under repeated 8- (Fig. 4(a)) and 9-J (Fig. 4(b)) impacts, similar to the damage analysis performed in previous studies [30–33], which analyzed the impact failure mechanism under multiple impacts.

The energy absorption and maximum displacement are measured during the repeated 8- and 9-J impact testing performed for investigating the failure mechanism during the repeated impact testing, as depicted in Fig. 5. At a low number of impacts, the indentation failure mechanism, which is caused mainly by matrix cracking and delamination, was observed. The locally compact area, which may decrease the energy absorption owing to an increase in the impact resistance caused by the compressed location, was investigated at the low number of impacts position. The indentation started at the first impact. As the composite was condensed by multiple impacts, the energy absorption decreased. However, it could not be infinitely compressed by impacts. Therefore, the energy absorption reached a steady state after approximately 10 impacts. Thereafter, the energy absorption started to increase with fiber breakage damages, that is, a more severe plastic deformation that may decrease the impact resistance. The energy absorption increased at the 25th and 23rd fiber breakage starting points indicated in Fig. 5(a) and 5(b), respectively. Beyond the fiber breakage start point, the maximum displacement increased more rapidly than that before the fiber breakage point. In the penetration damage state, the step impact energies of the 8- and 9-J impacts are totally absorbed, as indicated in Fig. 5(a) and 5(b), respectively; further, the maximum displacement is not increased in the penetration state.

The electrical-resistance-change ratio was estimated during repeated impacts to investigate the damage types and health status of the CFRP in real time. The electrical-resistance-change ratio at every impact is shown in Fig. 6.

Before the start of fiber breakage, the electrical-resistance-change ratio decreased as indicated in Fig. 6 because the indentation damage, where matrix cracking is dominant, exists in the CFRP, as depicted in Fig. 7(a)–(d), before the fiber breakage starting point. This leads to the compact electrical network in the CFRP; therefore, the electromechanical behavior reduces. The fiber breakage depicted in Fig. 6(a) and 6(b) causes electrical network breakage during the repeated impacts. The impact damage and fiber breakage in the CFRP become more severe with an increase in the number of impacts, as exhibited in Fig. 7(e)–(i). This causes the electrical network to break, which leads to an increase in the electromechanical behavior. The electrical-resistance-change ratio increases as the impact damage area is increased before the penetration damage states are reached. At the penetration damage state

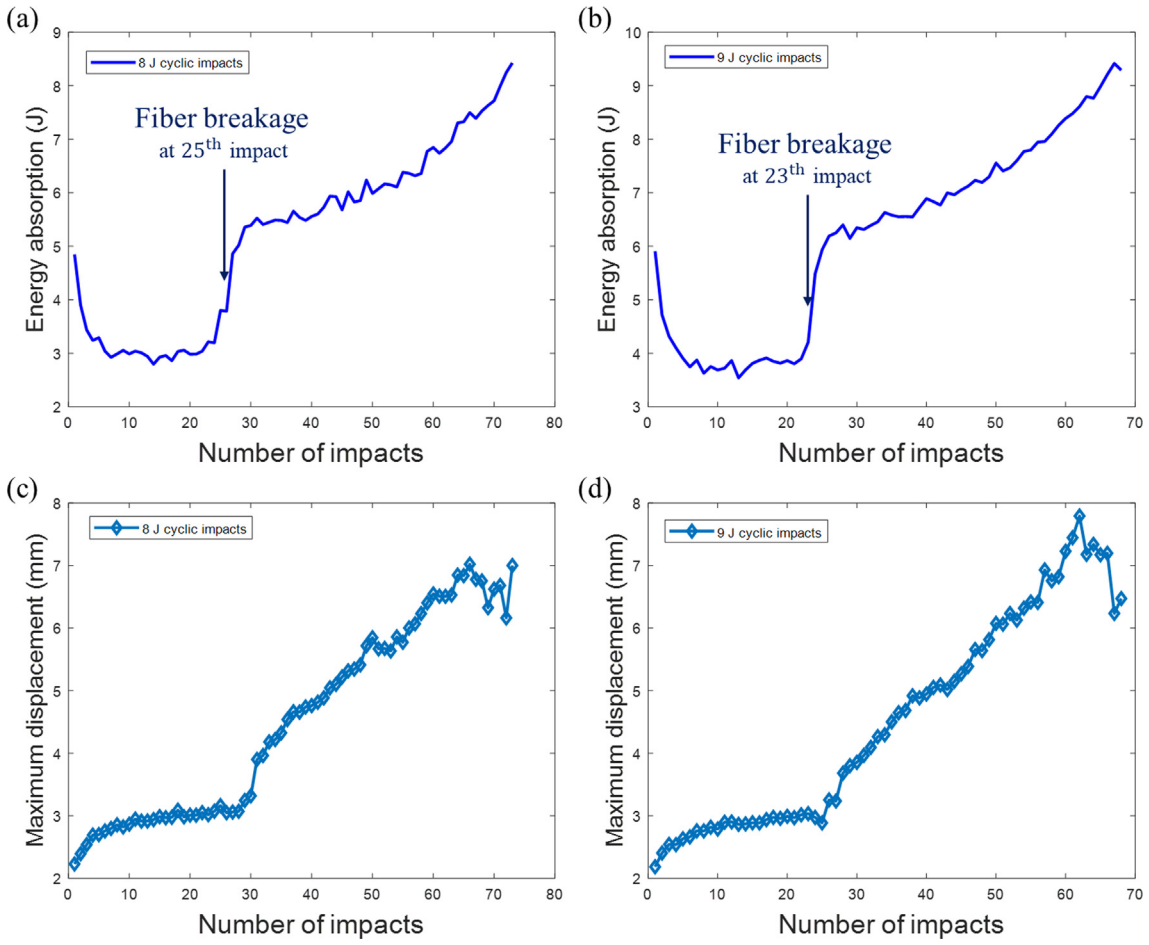

Fig. 5. Energy absorption graphs during (a) 8- and (b) 9-J repeated impacts and maximum displacement graphs with (c) 8 J and (d) 9 J under multiple impacts.

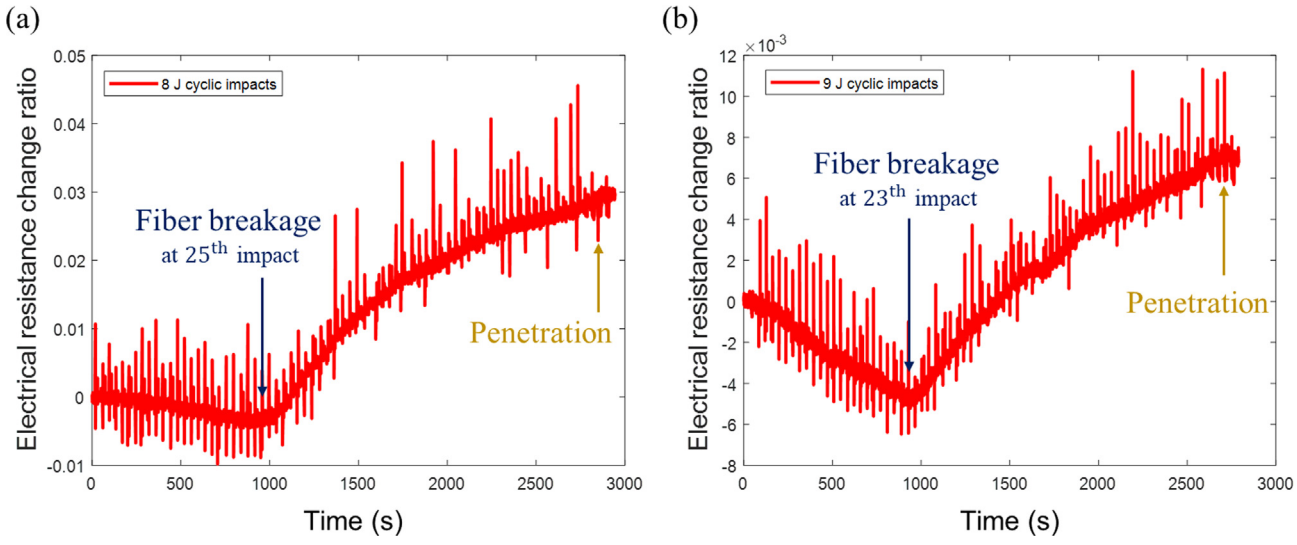

Fig. 6. Electrical-resistance-change ratio during the 8- and 9-J repeated impacts on CFRP.

depicted in Fig. 6, the electrical network breakage is not greater than that before because it was already totally penetrated, as exhibited in Fig. 7(j). Therefore, the electromechanical behavior does not change in this damage state. If significantly high multiple-impact energies were exerted on the CFRP, then the fiber breakage damage mechanism would occur at the first impact. This implies that a decreasing trend, which is mainly caused by indentation with delamination, in the electromechanical behavior cannot be demonstrated during multiple impacts; only an increasing trend in the electromechanical behavior can be illustrated during

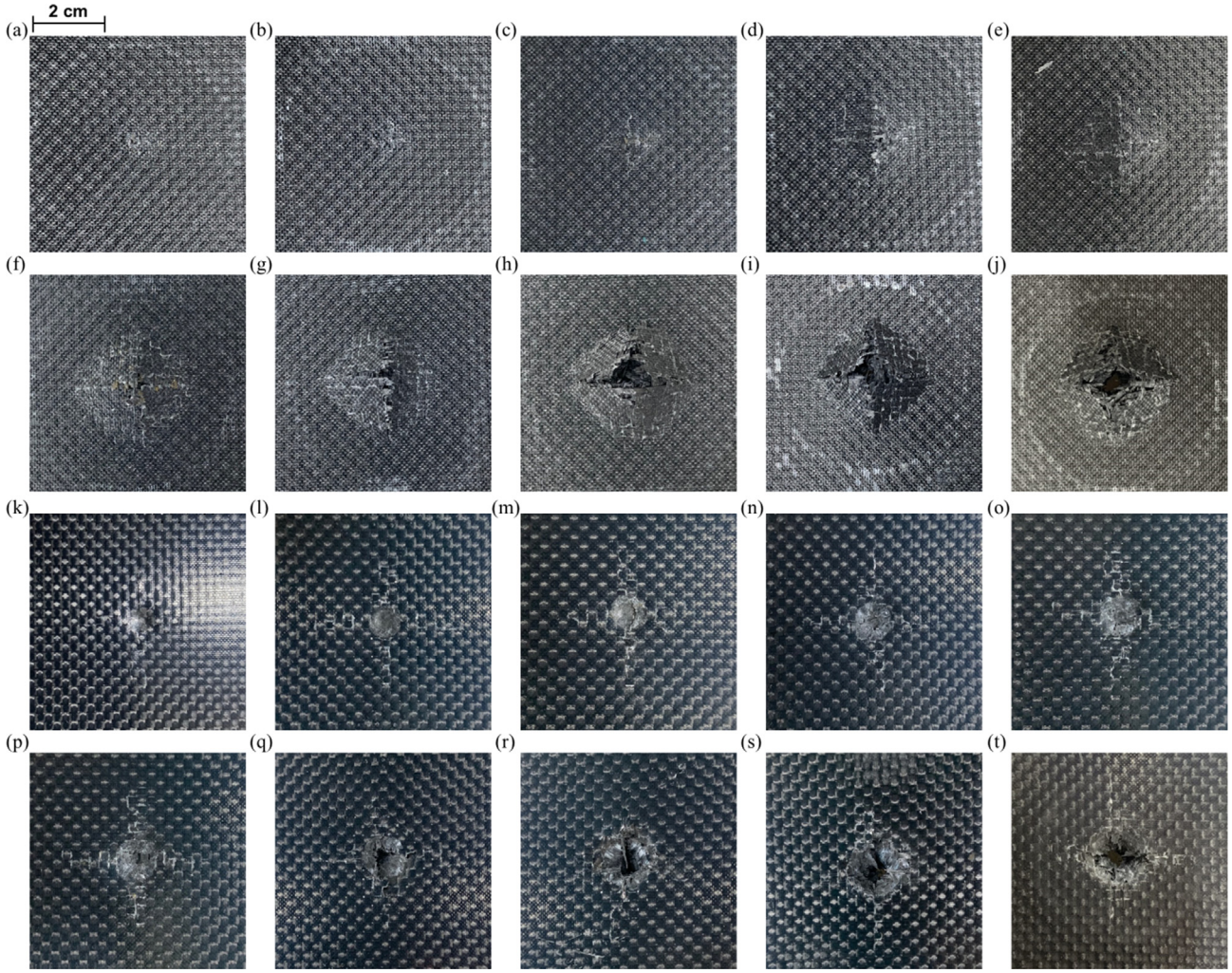

Fig. 7. Top view of the CFRP samples after (a) 1 impact, (b)–(i) 5, 10, 20, 30, 40, 50, 60, and 70 impacts, respectively, and (j) the last impact. Bottom view after (k) 1 impact, (l)–(s) 5, 10, 20, 30, 40, 50, 60, and 70 impacts, and (t) the last impact with 8 J of repeated impact energy.

multiple impacts. The current health and damage states could be observed in real time during repeated impact testing using the *in situ* electromechanical data.

The mechanical properties of the CFRP structures were measured and compared with the electromechanical behavior data in real time. Various damages such as delamination, matrix cracking (wherein the electrical-resistance-change ratio decreases), fiber breakage (wherein the electrical-resistance-change ratio increases), and penetration (wherein the electrical resistance is constant) were monitored in real time using the electrical resistance measurement under repeated impact testing. Further, the increase in the impact damage area was analyzed using self-sensing data. In this study, the behavior and failure mechanism exhibited by GFRP were similar to those exhibited by CFRP. However, GFRP cannot be monitored in real time using self-sensing because it has no electrical properties. The GFRP failure mechanism can be observed using self-sensing aided by carbon-nanomaterials in the same way as described in this study. Specimens with UD CFs instead of woven fibers also exhibited similar mechanical behavior and failure mechanisms under multiple impacts. Although the sensitivity against multiple impacts should vary based on the stacking sequence of the UD CF, the overall electromechanical behavior, which was reduced by the compact electrical network and improved by the electrical detour path with fiber breakage, is similar to that of the woven CF. The health status of the composites, impact damage accumulation, and damage severity could be observed and evaluated in real time using electromechanical behavior data.

3.2. PHM of CFRP

The electromechanical behavior was predicted based on the empirical self-sensing information for investigating the future health status of the CFRP using the PF. Furthermore, the remaining number of useful impacts was predicted and measured based on the prognostics analysis. When impacts were exerted with the same time interval between each impact, the degradation equations of electromechanical behavior were formulated considering repeated impact testing. Assuming that the change in time (Δt) is linearly proportional to the resistance-change ratio ($R_k - R_{k-1}$),

$$R_k = C^K(\Delta t) + R_{k-1} \tag{4}$$

Every prediction during repeated impacts with two different types of impact energies was conducted using Eq. (4) and the PF. A simple physical equation for the degradation reduced the computational calculation time and allowed it to be practical for the real-time prediction. All initial C^K standard deviation and average

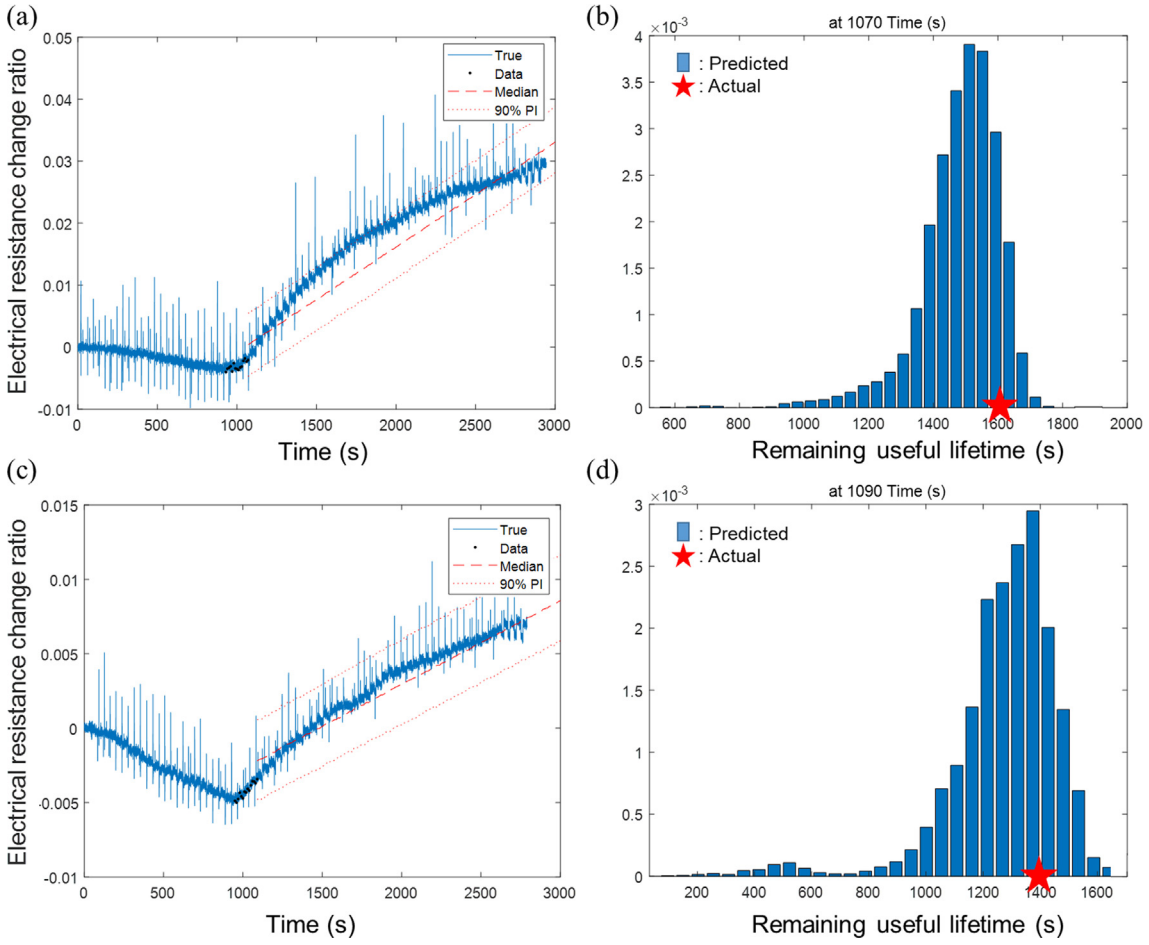

Fig. 8. Predicted electromechanical behavior during repeated impacts with (a) 8 J and (c) 9 J and calculated RUL with (b) 8 J and (d) 9 J.

values were 0.005 and 0, respectively. All electromechanical behaviors were predicted at the last point of data used for deciding the random variables in the PF algorithm.

The electromechanical behavior was predicted after the fiber breakage point. The predicted electromechanical behavior is presented in Fig. 8(a) and 8(c) with 8- and 9-J of repeated impact energies, respectively. The electromechanical behavior was well predicted in the 90% prediction internal (PI) range. The increasing trends in the electrical-resistance-change ratio were well prognosticated, which implies that damage accumulation and impact damage growth were well prognosticated. That is, the health state of the CFRP under repeated impact was well predicted in real time using the electromechanical behavior data and PF.

The RUL of the CFRP structures during repeated impact testing is calculated based on a probabilistic density function used for the prediction of the electromechanical behavior depicted in

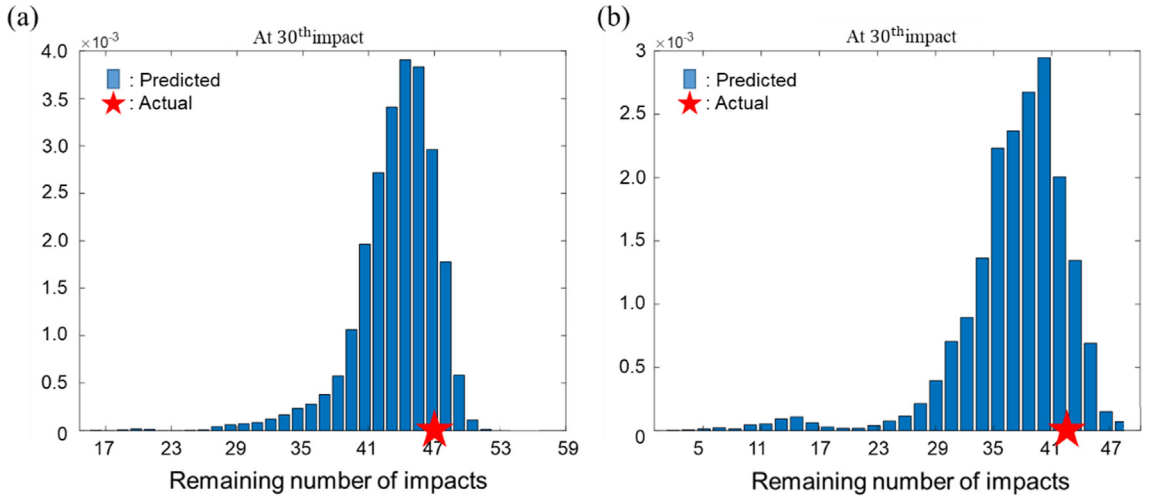

Fig. 9. Calculation of remaining number of useful impacts with (a) 8 J and (b) 9 J of repeated impact energies.

Fig. 8(b) and 8(d). Using the fact that multiple impacts were exerted on the CFRP in the time interval between each impact, the remaining number of useful impacts were calculated for 8 and 9 J of repeated impacts as indicated in Fig. 9(a) and (b). The estimated probabilistic remaining number of useful impact values for the CFRP with the 8- (43 times) and 9-J (38 times) impact specimens match well with their real remaining number of useful impact values (47 and 42 times, respectively). The standard deviations were 0.639 and 0.588, and the prognosis errors were 8.51% and 9.52% for the CFRP with 8- and 9-J impact energies, respectively.

Real-time PHM was investigated with real-time electromechanical data to prevent unexpected failure in the composite structures. The electromechanical behavior of CFRP that gradually increased under repeated impact was well predicted in the 90% PI in real time. Based on this prognostics analysis, damage accumulation, and material degradation during multiple impacts can be predicted. In addition, the remaining number of useful impacts was calculated using the probabilistic density function of the RUL in the self-sensing data measurement. The prediction results were estimated by the electromechanical behavior data during multiple impacts. It can indicate prior warnings about failure in composite structures and the impact damage growth and can be issued to raise warnings about the current and future health state of the composites during operation. Maximizing the life cycle and minimizing the unexpected maintenance cost of the CFRP structures are the expected effects by implementing the proposed CBM + based on the prediction results.

3.3. CBM + of scaled-down wind-turbine blade

To verify the applicability of the proposed CBM + methodology to 3D CFRP structures, repeated impact testing was performed to identify the damage, predict the electromechanical behavior, and calculate the remaining number of useful impacts in the carbon-fiber-based wind blade using its real-time self-sensing data measured for multiple 4- and 5-J impacts.

Fiber breakage started in the blade at the beginning of the impact. For a low number of impacts, the maximum displacement increased rapidly owing to the fiber breakage damage in the structures, as depicted in Fig. 10(b) and 10(d) under multiple 4- and 5-J impacts, respectively. A larger maximum displacement than those of the CFRP plate shape samples was observed because of the hollow shape of the blade. The displacement did not increase near the structural failure. However, energies up to 4 and 5 J were absorbed, which exerted a force on the CFRP wind blade, as depicted in Fig. 10(a) and 10(c).

Electrical resistance was observed in real time during the repeated impacts on the CFRP wind-turbine blade, and the change ratio of electrical resistance was calculated in Fig. 11(a) and 11(b) under two different multiple impacts. A total of 43 and 40 impacts were exerted on each CFRP wind blade. The resistance-change ratio increased rapidly with the start of the fiber breakage. Further, the electromechanical behavior improved gradually with an increase in the number of impacts, and the impact-damaged area increased because of the accumulation of impact damage. The structural failure of the wind blade occurred following the last impact. The

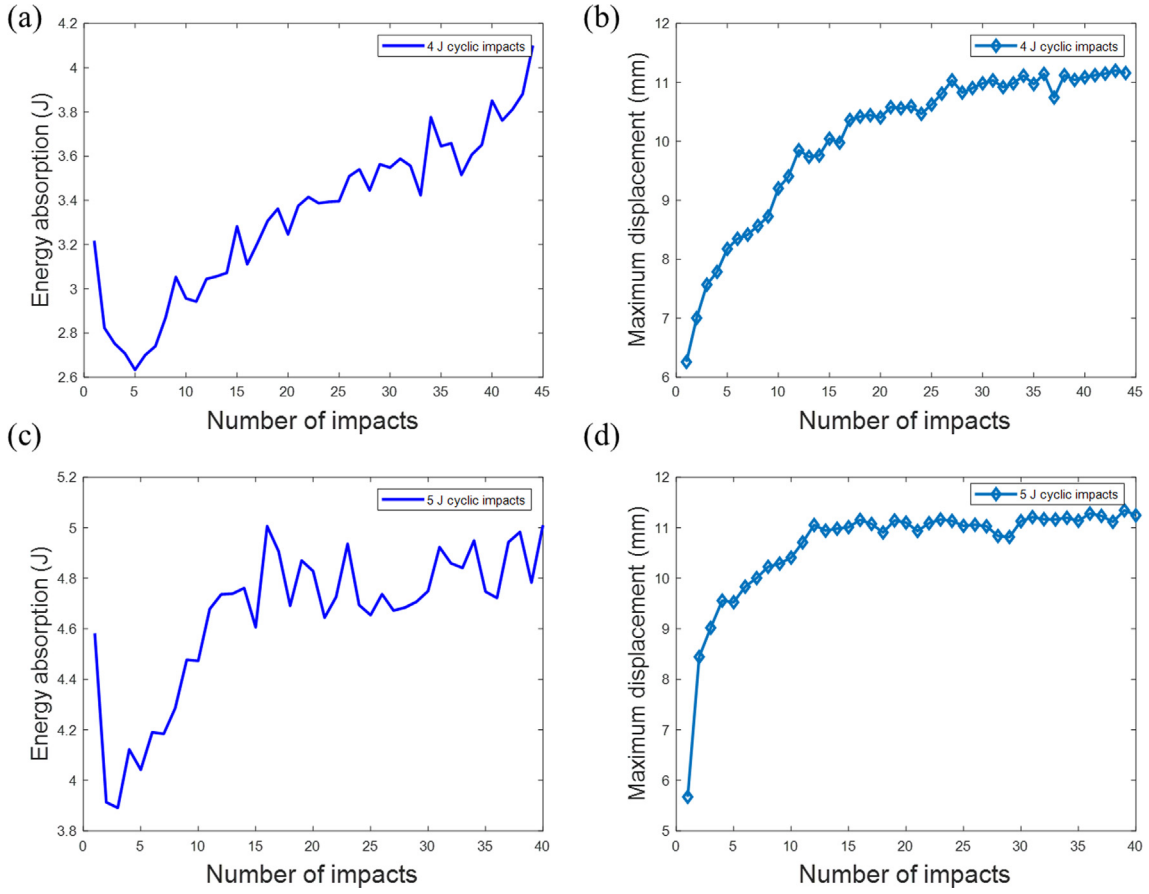

Fig. 10. (a) Energy absorption graph and (b) maximum displacement graph with multiple 4-J impacts; (c) energy absorption graph and (d) maximum displacement graph with multiple 5-J impacts in the wind-turbine blade.

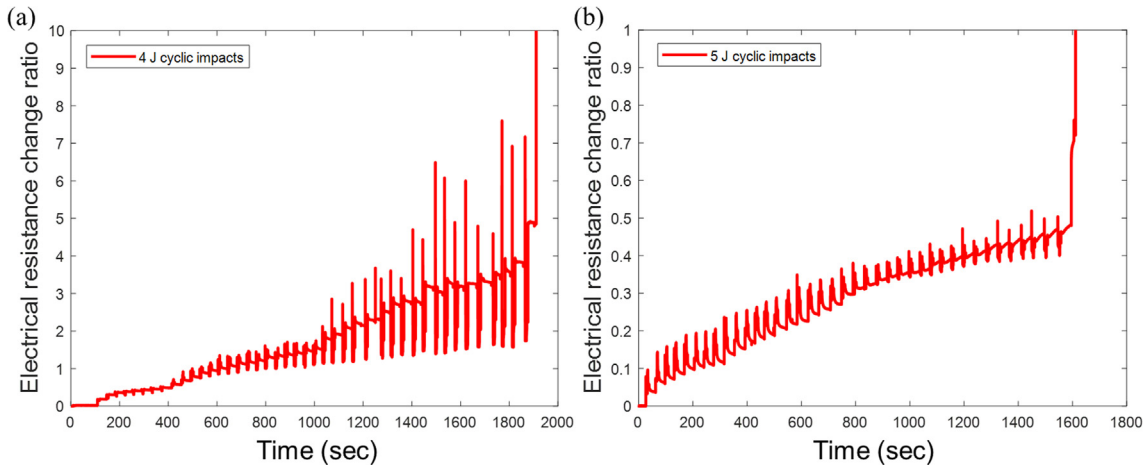

Fig. 11. Electromechanical behavior of CFRP wind-turbine blade under multiple (a) 4- and (b) 5-J impacts.

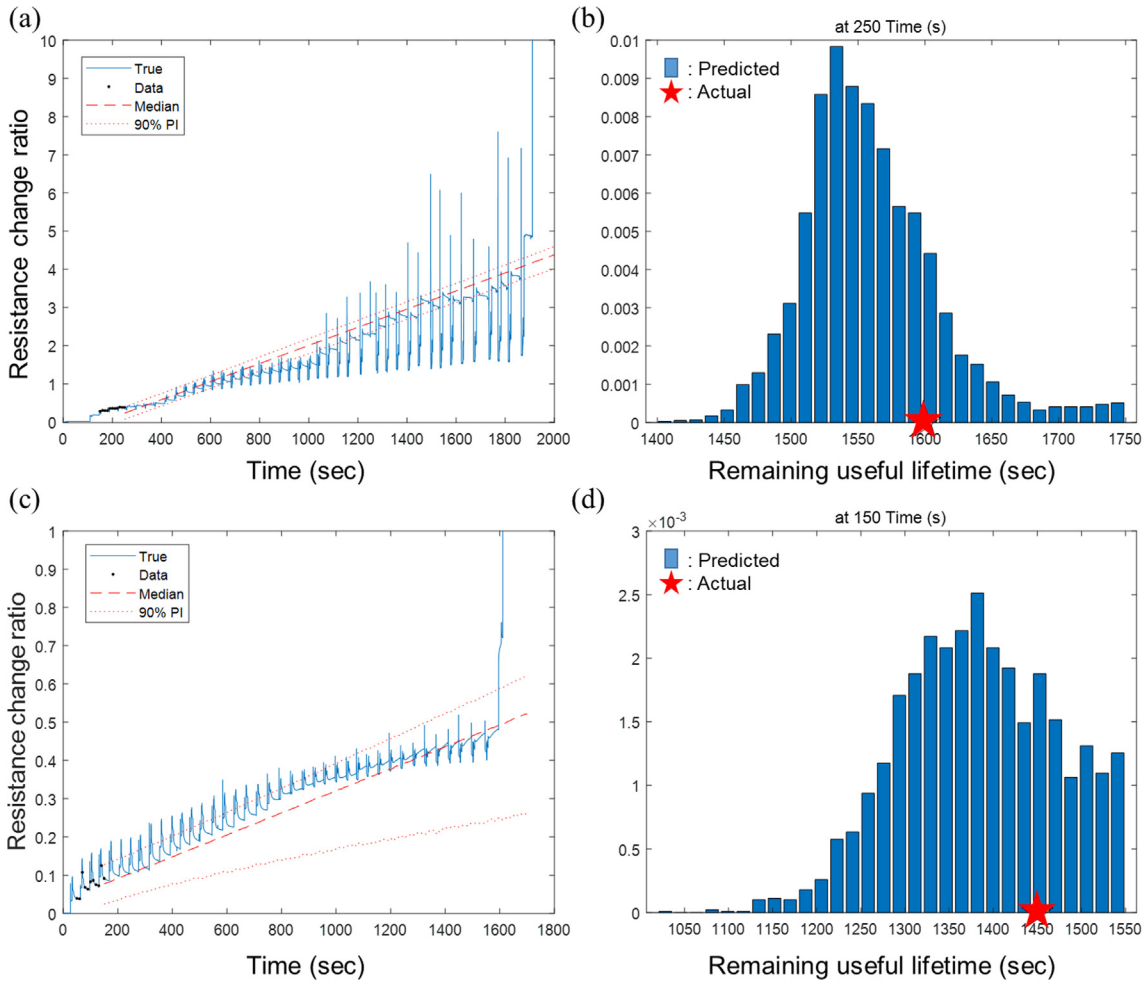

Fig. 12. Predicted electromechanical behavior during repeated impacts with (a) 4 and (c) 5 J; calculated RUL with (b) 4 J and (d) 5 J on a wind-turbine blade.

electrical-resistance-change ratio tends to infinity because of the fracture in the blade, which was divided into two parts. This is referred to as the general failure mechanism in the industry [4–6]. The health state of the wind blade, which includes failure modes, damage severity, and accumulation, can be analyzed in real time using real-time electromechanical behavior data. In addition, the fractures in the composite structures can be monitored.

The electromechanical behavior was predicted after the fiber breakage point using the PF and Eq. (4). The predicted electromechanical behavior under 4 and 5 J of repeated impact energy is presented in Fig. 12. The electromechanical behavior was well predicted in a 90% PI range. Further, the increasing trend in the electrical-resistance-change ratio was well prognosticated. This implies that damage accumulation and impact damage growth were well prog-

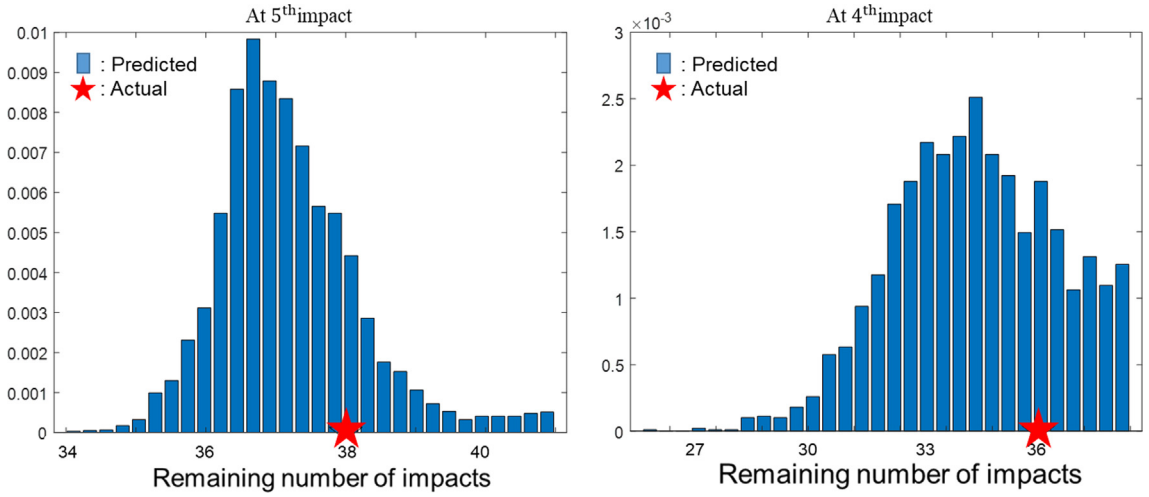

Fig. 13. Calculation of the remaining number of useful impacts with (a) 4 J and (b) 5 J of repeated impacts in the CFRP wind-turbine blade.

nosticated. That is, the health status of the CFRP wind blade under repeated impact was well predicted in real time using the electromechanical behavior data and PF. The RUL of the CFRP structures during repeated impact testing was calculated based on a probabilistic density function of the electromechanical behavior prediction presented in Fig. 12(b) and 12(d). Multiple impacts were performed on the blade in the same time interval between each impact. Thus, the remaining number of useful impacts was calculated under repeated impact, as depicted in Fig. 13. The calculated probabilistic remaining number of useful impact values for the wind blade with 4 J (37 times) and 5 J (34.5 times) agreed well with their actual remaining number of useful impact values (38 and 36 times, respectively). The standard deviations were 0.292 and 0.361, and the prognosis errors were 2.6% and 4.1% for the CFRP wind blade with multiple 4- and 5-J impacts, respectively.

Various damage types and the remaining number of useful impacts in 3D composites were analyzed in real time using self-sensing data and the PF algorithm. Owing to the large size of the wind-turbine blade (>60 m), manufactured using CF, it cannot be subjected to CEAST 9350 drop-weight impact testing. Therefore, the scaled-down blade was used to validate the applicability of the monitoring system. Condition-based monitoring along with the prognostics of the scaled-down wind blade, described in this paper, can be applied to various sizes of composite wind blades with similar structures. In addition, the glass-fiber-reinforced wind-turbine blade can be monitored and aided by carbon-nanomaterials. The current health states such as impact damage severity and accumulation in the blade could be observed in real time. Electromechanical behavior was predicted using the historical self-sensing data in real time. Material degradation during repeated impacts was well prognosticated. In addition, the remaining number of impacts was calculated within a 5% error. Ten impacts were exerted on the wind-turbine blades. All specimens exhibited similar electromechanical behavior and condition-based monitoring with prognostics analysis. The proposed CBM + can be utilized not only for wind blades but also for other carbon-fiber-based structures exposed to multiple impacts using their real-time electromechanical behavior data.

4. Conclusions

The proposed CBM + methodology for CFRP structures was used based on real-time electromechanical behavior data during repeated impact testing. The health status of the CFRP was observed using electromechanical data in real time. The PF was utilized to predict the electromechanical behavior and damage propagation during repeated impacts. The electromechanical behavior was well predicted in real time within a 90% PI. The health state of the CFRP including damage propagation and material degradation during repeated impacts could be prognosticated through prediction analysis. In addition, the remaining number of useful impacts was calculated within a 10% error.

Repeated impact testing was conducted on a CFRP wind-turbine blade in the same way as that for the plate-shaped CFRP, and the applicability of the proposed CBM + methodology for the 3D wind blade was verified. In future work, the electromechanical behavior and remaining number of useful impacts on composite structures should be predicted at various levels of multiple-impact energies and under random impact location conditions.

This paper proposed a real-time CBM + methodology that utilizes the electromechanical behavior data of composites. The damage analysis and prediction were investigated using electromechanical behavior. The failure mechanism under repeated impacts was analyzed. Further, the level of severity of the damages caused in the CFRP structures and the remaining number of impacts were estimated. This paper confirmed the applicability of the CBM + system to the analysis of the 3D shape of CFRP structures applied in a wide range of industries such as the aircraft and automobile industries. Furthermore, the component cost per electrode is $0.2, which is extremely cheaper compared with the cost of other sensor types or nondestructive evaluation (NDE) systems. The measuring equipment is relatively low-cost compared with other NDE methodologies. Therefore, installing electrodes on composite structures would not negatively affect the remaining life and total cost of the component. The proposed real-time condition-based maintenance methodology can improve maintenance decision making, increase the life cycle of the composite structure, reduce maintenance cost, increase system availability, and detect upcoming equipment failure. Thus, it is a more practical monitoring system when compared with other real-time NDE techniques.

Data availability

Data will be made available on request.

Declaration of Competing Interest

The authors declare that they have no known competing financial interests or personal relationships that could have appeared to influence the work reported in this paper.

Acknowledgments

This work was supported by the Basic Science Research Program (Mid-career Research Program, Grant No. NRF-2021R1A2C2009726) through the National Research Foundation of Korea (NRF) funded by the Ministry of Science and ICT of Korea.

Appendix A. Supplementary material

Supplementary data to this article can be found online at https://doi.org/10.1016/j.matdes.2022.111143.

References

[1] M. Jureczko, M. Pawlak, A. Mężyk, Optimisation of wind turbine blades, J. Mater. Process. Technol. 167 (2–3) (2005) 463–471.
[2] M. Rani, P. Choudhary, V. Krishnan, S. Zafar, A review on recycling and reuse methods for carbon fiber/glass fiber composites waste from wind turbine blades, Compos. B Eng. 215 (2021) 108768.
[3] K. Cox, A. Echtermeyer, Structural design and analysis of a 10MW wind turbine blade, Energy Procedia 24 (2012) 194–201.
[4] S. Asian, G. Ertek, C. Haksoz, S. Pakter, S. Ulun, Wind turbine accidents: a data mining study, IEEE Syst. J. 11 (3) (2016) 1567–1578.
[5] X. Chen, W. Zhao, X.L. Zhao, J.Z. Xu, Preliminary failure investigation of a 52.3 m glass/epoxy composite wind turbine blade, Eng. Fail. Anal. 44 (2014) 345–350.
[6] J.-S. Chou, W.-T. Tu, Failure analysis and risk management of a collapsed large wind turbine tower, Eng. Fail. Anal. 18 (1) (2011) 295–313.
[7] Y. He, G. Tian, M. Pan, D. Chen, Impact evaluation in carbon fiber reinforced plastic (CFRP) laminates using eddy current pulsed thermography, Compos. Struct. 109 (2014) 1–7.
[8] Y. He, G. Tian, M. Pan, D. Chen, Non-destructive testing of low-energy impact in CFRP laminates and interior defects in honeycomb sandwich using scanning pulsed eddy current, Compos. B Eng. 59 (2014) 196–203.
[9] C.S. Kumar, V. Arumugam, C. Santulli, Characterization of indentation damage resistance of hybrid composite laminates using acoustic emission monitoring, Compos. B Eng. 111 (2017) 165–178.
[10] Y.-H. Yu, J.-H. Choi, J.-H. Kweon, D.-H. Kim, A study on the failure detection of composite materials using an acoustic emission, Compos. Struct. 75 (1–4) (2006) 163–169.
[11] A. Datta, M. Augustin, N. Gupta, S. Viswamurthy, K.M. Gaddikeri, R. Sundaram, Impact localization and severity estimation on composite structure using fiber bragg grating sensors by least square support vector regression, IEEE Sens. J. 19 (12) (2019) 4463–4470.
[12] P. Ferdinand, S. Magne, V. Dewynter-Marty, S. Rougeault, L. Maurin, Applications of fiber Bragg grating sensors in the composite industry, MRS Bull. 27 (5) (2002) 400–407.
[13] S. Wang, D. Chung, J.H. Chung, Impact damage of carbon fiber polymer–matrix composites, studied by electrical resistance measurement, Compos. A Appl. Sci. Manuf. 36 (12) (2005) 1707–1715.
[14] S. Wang, D. Wang, D. Chung, J.H. Chung, Method of sensing impact damage in carbon fiber polymer-matrix composite by electrical resistance measurement, J. Mater. Sci. 41 (8) (2006) 2281–2289.
[15] Z.-J. Wang, D.-J. Kwon, G.-Y. Gu, H.-S. Kim, D.-S. Kim, C.-S. Lee, K.L. DeVries, J.-M. Park, Mechanical and interfacial evaluation of CNT/polypropylene composites and monitoring of damage using electrical resistance measurements, Compos. Sci. Technol. 81 (2013) 69–75.
[16] S. Wang, D. Chung, Self-sensing of flexural strain and damage in carbon fiber polymer-matrix composite by electrical resistance measurement, Carbon 44 (13) (2006) 2739–2751.
[17] J. Wen, Z. Xia, F. Choy, Damage detection of carbon fiber reinforced polymer composites via electrical resistance measurement, Compos. B Eng. 42 (1) (2011) 77–86.
[18] Y. Al-Assaf, H. El Kadi, Fatigue life prediction of composite materials using polynomial classifiers and recurrent neural networks, Compos. Struct. 77 (4) (2007) 561–569.
[19] H. Zamyad, N. Naghavi, R. Godaz, R. Monsefi, A recurrent neural network–based model for predicting bending behavior of ionic polymer–metal composite actuators, J. Intell. Mater. Syst. Struct. 31 (17) (2020) 1973–1985.
[20] Z. Zhang, K. Friedrich, Artificial neural networks applied to polymer composites: a review, Compos. Sci. Technol. 63 (14) (2003) 2029–2044.
[21] D.W. Abueidda, M. Almasri, R. Ammourah, U. Ravaioli, I.M. Jasiuk, N.A. Sobh, Prediction and optimization of mechanical properties of composites using convolutional neural networks, Compos. Struct. 227 (2019) 111264.
[22] C. Yang, Y. Kim, S. Ryu, G.X. Gu, Prediction of composite microstructure stress-strain curves using convolutional neural networks, Mater. Des. 189 (2020) 108509.
[23] A. Khan, D.-K. Ko, S.C. Lim, H.S. Kim, Structural vibration-based classification and prediction of delamination in smart composite laminates using deep learning neural network, Compos. B Eng. 161 (2019) 586–594.
[24] M.Y. Chiang, X. Wang, C.R. Schultheisz, J. He, Prediction and three-dimensional Monte-Carlo simulation for tensile properties of unidirectional hybrid composites, Compos. Sci. Technol. 65 (11–12) (2005) 1719–1727.
[25] M. Ngah, A. Young, Application of the spectral stochastic finite element method for performance prediction of composite structures, Compos. Struct. 78 (3) (2007) 447–456.
[26] T. Okabe, N. Takeda, Y. Kamoshida, M. Shimizu, W.A. Curtin, A 3D shear-lag model considering micro-damage and statistical strength prediction of unidirectional fiber-reinforced composites, Compos. Sci. Technol. 61 (12) (2001) 1773–1787.
[27] P. Banerjee, O. Karpenko, L. Udpa, M. Haq, Y. Deng, Prediction of impact-damage growth in GFRP plates using particle filtering algorithm, Compos. Struct. 194 (2018) 527–536.
[28] P. Zhu, Y. Cheng, P. Banerjee, A. Tamburrino, Y. Deng, A novel machine learning model for eddy current testing with uncertainty, NDT and E Int. 101 (2019) 104–112.
[29] P. Banerjee, R.P. Palanisamy, L. Udpa, M. Haq, Y. Deng, Prognosis of fatigue induced stiffness degradation in GFRPs using multi-modal NDE data, Compos. Struct. 229 (2019) 111424.
[30] B.M. Icten, Repeated impact behavior of glass/epoxy laminates, Polym. Compos. 30 (11) (2009) 1562–1569.
[31] B. Liao, J. Zhou, Y. Li, P. Wang, L. Xi, R. Gao, K. Bo, D. Fang, Damage accumulation mechanism of composite laminates subjected to repeated low velocity impacts, Int. J. Mech. Sci. 182 (2020) 105783.
[32] M.V. Hosur, M.R. Karim, S. Jeelani, Experimental investigations on the response of stitched/unstitched woven S2-glass/SC15 epoxy composites under single and repeated low velocity impact loading, Compos. Struct. 61 (1–2) (2003) 89–102.
[33] E. Sevkat, B. Liaw, F. Delale, B.B. Raju, Effect of repeated impacts on the response of plain-woven hybrid composites, Compos. B Eng. 41 (5) (2010) 403–413.
[34] L. Torre, J.M. Kenny, Impact testing and simulation of composite sandwich structures for civil transportation, Compos. Struct. 50 (3) (2000) 257–267.
[35] Y. Chen, S. Hou, K. Fu, X. Han, L. Ye, Low-velocity impact response of composite sandwich structures: modelling and experiment, Compos. Struct. 168 (2017) 322–334.
[36] F.M. Jensen, B.G. Falzon, J. Ankersen, H. Stang, Structural testing and numerical simulation of a 34 m composite wind turbine blade, Compos. Struct. 76 (1–2) (2006) 52–61.
[37] M.M. Shokrieh, R. Rafiee, Simulation of fatigue failure in a full composite wind turbine blade, Compos. Struct. 74 (3) (2006) 332–342.
[38] I.Y. Lee, H.D. Roh, H.W. Park, Y.B. Park, Advanced non-destructive evaluation of impact damage growth in carbon-fiber-reinforced plastic by electromechanical analysis and machine learning clustering, Compos. Sci. Technol. 218 (2022) 109094.